SAN FRANCISCO ESTUARY & WATERSHED SCIENCE
Sponsored by the Delta Science Program and UC Davis Institute for the Environment

RESEARCH

The Flood Risk and Water-Supply Implications of Seasonal Precipitation Reconstructions in Northern California

Ian M. Howard*[1], David W. Stahle[1], Max C. A. Torbenson[2], Daniela Granato–Souza[1], Cody Poulsen[3]

ABSTRACT

Subsets of annual and sub-annual tree-ring chronologies are used to reconstruct seasonal precipitation totals in northern California. The specific seasons selected for reconstruction are based on the strongest monthly precipitation signals recorded in the tree-ring data. Earlywood width of gray pine is best correlated with Oct–Dec precipitation at the onset of the wet season. Latewood width of ponderosa pine is correlated with Mar–Apr totals at the end of the wet season. These earlywood and latewood width chronologies are used to develop separate reconstructions of precipitation for the "autumn" (Oct–Dec) and "spring" (Mar–Apr) seasons. Total ring-width chronologies of blue oak are highly correlated with October–April precipitation totals and are used to reconstruct precipitation for the "wet season." We then computed one additional skillful reconstruction by subtracting the reconstructed spring totals from the wet season precipitation estimates (i.e., "winter" [Oct–Feb]). We compare the winter and spring reconstructions because they are well calibrated and provide an interesting long-term perspective on the interaction of winter–spring precipitation amounts near March 1, when important reservoir management decisions are often made. Consecutive wet winter and very wet spring precipitation anomalies increased after 1950 in the instrumental and reconstructed time-series, often coinciding with the largest spring streamflow and flood events recorded on the American River at Folsom. Once the sub-annual tree-ring data can be improved, it may be possible to develop discrete reconstructions of early-, middle-, and late-season precipitation for the past 250 to 500 years, to help define natural variability and anthropogenic forcing of seasonal precipitation totals in California.

SFEWS Volume 21 | Issue 1 | Article 2

https://doi.org/10.15447/sfews.2023v21iss1art2

* Corresponding author: ihowardksu@gmail.com

1 Department of Geosciences
University of Arkansas
Fayetteville, AR 72730 USA

2 Department of Geography
Johannes Gutenberg University
55099 Mainz, Germany

3 Center for Western Weather and Water Extremes
Scripps Institution of Oceanography
La Jolla, CA 92093 USA

KEY WORDS

Pinus ponderosae, Pinus sabiniana, Quercus douglasii, seasonal precipitation reconstructions, tree rings, atmospheric rivers, paleoclimatology

INTRODUCTION

The variability of seasonal to sub-seasonal precipitation can influence flood risk and water supply in California. Approximately 80% to 90% of annual precipitation occurs during the wet season from October through April (Cayan and Roads 1984), but precipitation in autumn, winter, and spring can have distinct environmental and water-resource effects. The onset of the wet season in autumn can greatly reduce wildfire hazards (Williams et al. 2019; Goss et al. 2020). Sierra Nevada snowpack accumulated in winter provides the main source of water for agriculture and hydropower in California (Bales et al. 2006). Spring precipitation represents the smallest seasonal fraction of average wet season totals, but major spring storms can augment water supplies in some otherwise dry years. The correlation between autumn, winter, and spring precipitation is low, but the variability of precipitation totals in each of these seasons is governed by just a handful of large storm events each year (Dettinger 2013, 2016; Lamjiri et al. 2018). These heavy storm totals are frequently delivered via landfalling atmospheric rivers (ARs) and can have a large influence on water supply and flood risk across the western US (Dettinger 2013).

Analyses of instrumental precipitation data in California indicate increased variability (Granger 1979), delayed onset of the wet season, and significant drying trends in autumn and spring since the mid 20th century (Swain et al. 2018; Goss et al. 2020; Luković et al. 2021). Climate model projections of shoulder season precipitation suggest that autumn and spring drying will occur in the 21st century, while winter is projected to become wetter as the result of an increase in the frequency and magnitude of extreme storms (Neelin 2013; Polade et al. 2017; Swain et al. 2018). Wetter winters coupled with drier and warmer conditions during spring could affect the timing of snowmelt and runoff, which could affect reservoir operations and water rights, and might be detrimental to riparian ecosystems (Willis et al. 2011; Schwartz et al. 2017).

Reservoir management in California attempts to balance flood risk with water supply, and is dictated by seasonal rule curves that set the maximum amount of water that can be stored in a reservoir for each day of the year (Howard 1999; Willis et al. 2011). These rule curves are based on average seasonal precipitation and runoff, and require more empty reservoir space during the flood-prone winter season. Once monthly mean precipitation begins to decline in spring, reservoir operators may capture storm runoff for water supply. The rate of reservoir refill during spring can be determined in part by the antecedent winter conditions, with the highest rate of spring refill allowed after a dry winter (Willis et al. 2011). Reservoir management in California is therefore sensitive to precipitation and runoff from winter to spring, but the rule curves used are based on limited historical precipitation data and may not represent the full range of variability in winter and spring precipitation. Long-proxy reconstructions of seasonal precipitation could help define natural variability and the frequency of co-occurring seasonal extremes, a potentially useful historical perspective for water resource managers.

Several climate-sensitive tree species have been used for tree-ring chronology development and hydroclimatic reconstruction across western North America (e.g., Cook et al. 1999; Meko et al. 1980; Meko and Woodhouse 2005; Griffin and Anchukaitis 2014; Stahle et al. 2020; Wise 2020; Woodhouse et al. 2020; Williams et al. 2021). These reconstructions are largely based on chronologies of total ring width (RW) that tend to integrate climate across several months during and preceding the tree growth season, resulting in reconstructions of climate variables like the Palmer Drought Severity Index (Cook et al. 1999; Meko et al. 1980), annual precipitation (Michaelsen et al. 1987), and annual streamflow totals (Meko et al. 2001). Subsets of tree-ring chronologies with cool (Dec–Apr) and warm (May–Jul) season precipitation signals have recently been used to develop the gridded North American Seasonal Precipitation Atlas (NASPA; Stahle et al. 2020), but the NASPA reconstructions were not able to isolate the early, middle, or late wet-season precipitation totals in California. Wise (2020) used the available network of tree-ring

chronologies to reconstruct precipitation and runoff for separate months and seasons over the US West Coast, which is possible because some RW chronologies embed a stronger sub-annual signal even though they are also correlated with precipitation at longer inter-seasonal time-scales (i.e., the full wet season or even the water year; St. George et al. 2010). RW chronologies from the western US have also proven to be useful proxies for the number of ARs that make landfall during the cool season each year (Steinschneider et al. 2018; Borkotoky et al. 2021).

Sub-annual tree-ring chronologies of earlywood (EW) and latewood (LW) width can be used to estimate discrete meteorological and climate conditions at daily, monthly, and seasonal time-scales (Stahle et al. 2009; Griffin et al. 2013; Watson and Luckman 2016; Carlón–Allende et al. 2018; Howard and Stahle 2020; Stahle et al. 2020; Ziaco 2020). However, the availability of EW and LW width chronologies is still limited, and it is unclear if sub-annual ring-width data can be used in California to narrow the window of climate reconstruction down to seasonal or possibly sub-seasonal time-scales to provide insight into precipitation variability and extremes.

In this study, we develop sub-annual tree-ring chronologies from gray pine (*Pinus sabiniana*) and ponderosa pine (*Pinus ponderosae*) located in northern California. We use monthly response analyses to illustrate the autumn (Oct–Dec) precipitation signal in select gray pine EW chronologies and a spring (Mar–Apr) precipitation signal in ponderosa pine adjusted latewood width chronologies (LWa, adjusted to remove the correlation with EW growth; Meko and Baisan 2001). We use these specific seasonal precipitation signals in the gray pine EW and ponderosa pine LWa chronologies to separately reconstruct autumn and spring precipitation. We also compute a wet season (Oct–Apr) reconstruction from the strong wet season precipitation signal in four RW chronologies of blue oak (*Quercus douglasii*). We then use the wet season and spring reconstructions to calculate precipitation estimates for a long "winter" season (Oct–Feb) by subtracting the spring precipitation totals from the full wet season reconstruction. We then investigate the interannual and decadal variability in seasonal precipitation, and the interaction of winter and spring precipitation extremes, using both the instrumental and reconstructed time-series.

METHODS AND DATA

Study Area and Tree-Ring Chronology Development

Several new tree-ring chronologies of gray pine and ponderosa pine were used in this study along with four existing blue oak collections (Figure 1, Table 1). Gray pine is a California endemic species that often co-occurs with blue oak in the foothills of the Coast Ranges and Sierra Nevada near the lower forest border, where warm and dry conditions favor extreme growth sensitivity to precipitation (Powers 1990). The species can likely live for 300 years, but many existing gray pine stands appear to be much younger, and the species has not been previously used for dendroclimatology. Ponderosa pine is widespread in California and was used in A.E. Douglass' first scientific article on dendroclimatology (Douglass 1909). Blue oak chronologies are highly correlated with wet season precipitation totals, and have been widely used for hydroclimatic reconstructions in California (Stahle et al. 2001; St. George et al. 2010; Meko et al. 2011; Stahle et al. 2013; Belmecheri et al 2016).

The annual growth rings on all core specimens were exactly dated with dendrochronology. The width of the EW and LW components of the annual ring were measured separately to a precision of 0.001 mm and were then summed for total ring width. The methods outlined by Stahle et al. (2009) were used to delineate the earlywood and latewood boundaries in each growth ring. The measured ring-width series of EW, LW, and RW were detrended using a cubic smoothing spline with a 0.50 frequency response at a wavelength equal to 70% of each measured series (Cook and Peters 1981). We average the growth indices into the respective EW, LW, and RW index chronology using the robust mean-value function (Cook 1985). We then used autoregressive modeling (Meko 1981) to remove

https://doi.org/10.15447/sfews.2023v21iss1art2

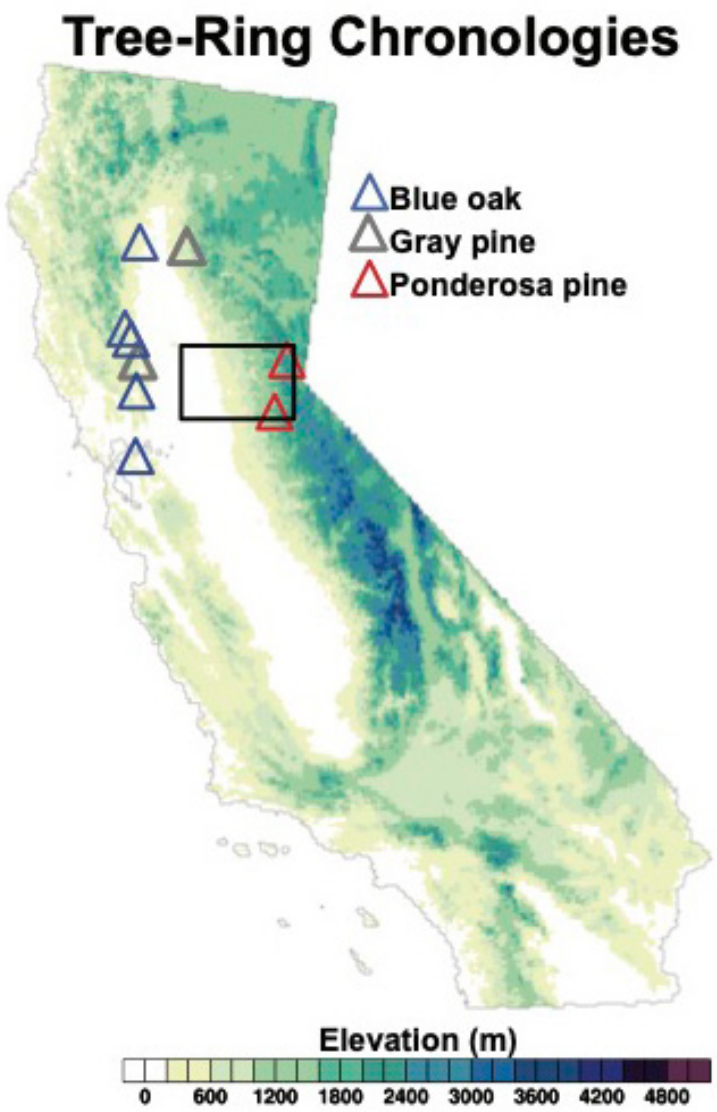

Figure 1 (**A**) The tree-ring collection sites are mapped and the study area in northern California is outlined (38.5–39.5ºN, 122–120ºW). The tree-ring data include earlywood (EW) and latewood (LW) chronologies of gray pine and ponderosa pine. Total ring-width (RW) chronologies of blue oak were used in the reconstruction of wet season (Oct–Apr) precipitation and to derive estimates of winter (Oct–Feb) precipitation.

Table 1 The tree-ring collection sites are identified along with the species sampled, location, elevation, and length of the derived chronology. The species abbreviations are ponderosa pine (PIPO), gray pine (PISB), and blue oak (QUDG). Earlywood (EW), latewood (LW), and total ring-width (RW) chronologies were developed for the conifers, while only RW chronologies were available for blue oak. The number of radii sampled and used in the calculation of the EW, LW, and RW chronologies is listed for all species.

Site name	Species	Latitude	Longitude	Elevation (m)	Length	Sample size
Bear River Ridge	PIPO	38.54	120.35	1710	1680-2017	48
Truckee River	PIPO	39.28	120.25	1890	1750-2017	41
Finley Lake	PISB	40.27	121.85	854	1771-2018	24
Walker Ridge	PISB	39.03	122.44	535	1897-2017	31
Clear Lake	QUDG	39.02	122.82	426	1620-2004	102
Bear Valley Buttes	QUDG	39.21	122.44	490	1546-2004	42
Mount Diablo	QUDG	37.87	121.95	245	1645-2003	84
Putah Creek	QUDG	38.67	122.27	180	1534-2004	35

the autocorrelation present in each chronology, to produce the persistence-free "residual" chronologies that were used to correlate with the instrumental precipitation data. We used the Kalman filter (Welch and Bishop 2006) to compute the ponderosa pine data for LWa chronologies, which represent LW growth that is not correlated with antecedent EW growth (Meko and Baisan 2001). Previous studies have shown that RW of ponderosa pine from California is correlated with precipitation late in the wet season (Johnson et al. 2017; Finley and Zhang 2019), and this signal can be enhanced using just the LW component of the annual ring (see Figure 2B). However, the LW width chronology shares a significant co-variability with EW width and precipitation before spring. We hypothesized that regressing the LW width chronology on the EW chronology would result in a residual time-series with a late-season precipitation signal not well correlated with moisture during the prior months. This method is similar to what is applied to EW and LW conifer chronologies in the southwestern US, where LW regression on the EW chronology produces a time-series that can enhance the summer precipitation signal (Meko and Baisan 2001; Stahle et al. 2009; Griffin et al. 2013).

Instrumental Precipitation and Integrated Vapor Transport Data

We extracted and averaged gridded instrumental precipitation data for a study area in northern California (38°–39.5°N, 122°–120°W; Figure 1). We chose this region because the various blue oak, gray pine, and ponderosa pine chronologies are most highly correlated with seasonal precipitation in this area. We then used these regional precipitation data for daily and monthly precipitation response analyses, calibration of the seasonal tree-ring reconstructions, and analyses of seasonal precipitation variability. We acquired daily precipitation data from the National Oceanic and Atmospheric Administration (NOAA) Climate Prediction Center's (CPC) US Unified Gauge-Based Analysis of Precipitation data set (Higgins et al. 2000, 2007). The gridded daily data cover the continental US at 0.25° latitude by 0.25° longitude resolution from 1948 to the present. The daily totals at each grid point are calculated for the 24-hour period ending at 1200 UTC of the current day. Monthly precipitation data from the Global Precipitation Climatology Centre (GPCC; Schneider et al. 2022) were also used to examine the distribution of seasonal precipitation totals and the relationship between winter and spring precipitation over the full instrumental period from 1891 to 2016. Monthly precipitation data from the parameter-elevation regression on independent slopes model (PRISM) climate group (Daly et al. 1994) were used to illustrate the spatial correlation patterns between the seasonal tree-ring reconstructions and the respective seasonal precipitation data. Gridded 3-hourly integrated vapor transport (IVT) data from MERRA-2 (Gelaro et al. 2017) were used to examine the connections between seasonal AR variability and the instrumental and reconstructed seasonal precipitation totals for the study area (based on 1980 to 2003 for winter, and 1980 to 2017 for autumn and spring).

Calibration and Verification of the Seasonal Precipitation Reconstructions

Seasonal Definitions

We used the EW chronologies of gray pine to reconstruct autumn precipitation (Oct–Dec), the full RW chronologies of blue oak to reconstruct wet season precipitation (Oct–Apr), and the LWa width chronologies of ponderosa pine to reconstruct spring precipitation totals (Mar–Apr) in the northern California study area. We then used the winter and spring reconstructions to derive one additional tree-ring-based estimate of "winter" precipitation (Oct–Feb). The autumn, wet season, and winter reconstructions are not independent because of the shared monthly totals, but are based on different tree species, and are computed to simply demonstrate feasibility for the reconstruction of sub-wet-season totals. We used these specific seasons because they represent the strongest precipitation signal detected in the available EW, LWa, and RW chronologies. Only the winter (Oct–Feb) and spring (Mar–Apr) reconstructions are analyzed in detail.

https://doi.org/10.15447/sfews.2023v21iss1art2

Seasonal Reconstructions

We used the full time-interval in common to the CPC instrumental precipitation and tree-ring data to calibrate the autumn, wet season, and spring reconstructions. To test the stability of the relationships between the reconstructions and the instrumental data, we also computed split calibration and validation experiments on early (1948 to 1982 for autumn and spring; 1949 to 1976 for the wet season) and late time-periods (1983 to 2017 for autumn and spring; 1977 to 2003 for the wet season). We computed an additional independent validation using the GPCC data by correlating the reconstructions with the respective instrumental seasonal precipitation data from 1900 to 1947 (autumn and winter) and 1900 to 1948 (wet season). The validation statistics include the Pearson correlation coefficient, reduction of error, and coefficient of efficiency (Table 2; Cook and Kairiukstis 1990).

We computed the reconstruction of autumn precipitation using an average of the Finley Lake and Walker Ridge gray pine EW width chronologies and calibrated on power-transformed autumn precipitation totals for the period 1948 to 2017. We used the Box-Cox power transformation method (Box and Cox 1964) to reduce the positive skewness of the instrumental data. After calibration, we back-transformed the reconstructed estimates into the original units of winter precipitation.

We used four blue oak RW chronologies (Table 1) to calculate the wet season precipitation reconstruction. We used stepwise regression using the individual chronologies, which resulted in markedly improved calibration statistics compared to bivariate or principal component regression approaches. We calibrated the reconstruction with the wet-season instrumental precipitation data over the full common period of 1949 to 2003 (the available blue oak chronologies were not updated to present for this study)

We constructed the spring precipitation totals using the average of two ponderosa pine LWa chronologies as the single predictor variable in a bivariate regression model (i.e., Bear River Ridge and Truckee River; Tables 1 and 2). We calibrated the LWa chronology on log-transformed spring precipitation data from 1948 to 2017. We then back-transformed the spring estimates to the original units of precipitation by taking the exponent of the reconstructed values.

We computed the winter precipitation reconstruction (Oct–Feb) by subtracting the spring reconstruction (Mar–Apr) from the wet-season reconstruction. We then re-scaled the derived winter estimates to the instrumental winter precipitation data. We used correlation analysis to document the agreement between the winter reconstruction and the instrumental totals for the common period of 1949 to 2003 and for an independent verification period of 1900 to 1948. For all reconstructions, we restored the instrumental variance lost in regression, and used the instrumental data to extend the records to 2022.

Daily Correlation Analysis

If the tree-ring reconstructions are to be used to compare the interaction of seasonal extremes, it is important to determine if the tree-ring estimates have discrete seasonal signals. Daily correlation analyses were used to demonstrate the separate seasonal precipitation signals embedded in the tree-ring reconstructions (e.g., Jevšenak 2019; Howard and Stahle 2020). The daily precipitation data for the study area were first summed for three intervals based on the length of the seasonal precipitation variable (i.e., 60 days spring, 90 days for autumn, 150 days for winter, and 210 days for the wet season) advancing one day at a time from the prior October 1 to the current September 30. The correlation coefficients for the 60-, 90-, 150-, and 210-day sums are plotted for the last day of each period, such that the correlation value on October 1 for a 60-day sum (represents the period from August 2 to October 1). This produces 365 annual time-series for each year and seasonal sum that could then be correlated with the tree-ring chronologies or reconstructions to determine the optimal season of precipitation response. We then used the calculated correlation coefficients for each interval and day of the year to plot daily response profiles. We also correlated instrumental seasonal

Table 2 Calibration and verification statistics are listed for the seasonal precipitation reconstructions. The autumn (Oct–Dec), wet season (Oct–Apr), and spring (Mar–Apr) precipitation reconstructions were calculated using the full calibration period in common with the instrumental data, but split period calibration and verification statistics are also listed. Each reconstruction was also correlated with independent instrumental precipitation data (using GPCC) from 1900 to 1947 for the autumn and spring reconstructions and 1900 to 1948 for the wet season and winter reconstructions. The R^2adj is the explained variance during the calibration period adjusted for the loss of degrees of freedom, RE is the reduction of error and CE the coefficient of efficiency statistic both computed for the verification interval, and r is Pearson correlation coefficient. Note that the calibration of the wet season reconstruction begins in 1949 because autumn precipitation totals from 1948 are summed with Jan-Apr precipitation totals in 1949. The transfer functions used to calculate the reconstructions are included below each variable (pt = power transformed). $X1_t$ to $X4_t$ for the wet season reconstruction are the RW chronology values in year t for Mt. Diablo, Bear Valley Buttes, Putah Creek, and Clear Lake, respectively.

Variable	Calibration	Verification	R^2adj	RE	CE	r
1. Autumn (Oct–Dec)	1948-1982	1983-2017	0.49	0.33	0.33	0.60
$pt\hat{Y}t = 7.212 + 10.159X$	1983-2017	1948-1982	0.34	0.48	0.48	0.71
	1948-2017	—	0.43	—	—	—
	—	1900-1947	—	—	—	0.54
2. Wet season (Oct–Apr)	1949-1976	1977-2003	0.85	0.68	0.68	0.88
$\hat{Y}t = 420.2 + 0.825X1_t + 0.614X2_t + -0.507X3_t + -0.349X4_t$	1977-2003	1949-1976	0.80	0.67	0.67	0.84
	1949-2003	—	0.79	—	—	—
	—	1900-1948	—	—	—	0.76
3. Spring (Mar–Apr)	1948-1982	1983-2017	0.53	0.54	0.53	0.78
$\log\hat{Y}_t = 5.352 + 0.735X$	1983-2017	1948-1982	0.60	0.41	0.40	0.73
	1948-2017	—	0.56	—	—	—
	—	1900-1947	—	—	—	0.60
4. Winter (Oct–Feb)	1949-2003	—	—	—	—	0.82
	—	1900-1948	—	—	—	0.70
Midwinter (Jan–Feb)	1949-2003	—	—	—	—	0.57
	—	1900-1948	—	—	—	0.43

precipitation totals with the daily precipitation data to compare how well the response profiles of the seasonal reconstructions matched the response profiles of the instrumental data. The daily correlation analyses were based on 1948 to 2017 for autumn and spring, and on 1949 to 2003 for the wet season and winter estimates.

RESULTS

Monthly Precipitation Response of the EW, LW, and Adjusted LW Chronologies

To illustrate the autumn and spring precipitation signals present in these sub-annual proxies, we correlated the gray pine EW and ponderosa pine LWa width chronologies with monthly precipitation totals from the northern California study area for all 12 months of the year. The gray pine EW width chronology—based on the average of the Finley Lake and Walker Ridge chronologies—is most highly correlated with precipitation in autumn and early winter (Figure 2A). The regional gray pine LW width chronology is significantly correlated with precipitation during all months of the wet season, peaking in March and April (Figure 2A). Adjusted gray pine LW width chronology has no detectable seasonal precipitation signal.

The ponderosa pine EW width chronology does not have a strong precipitation signal during the wet season (Figure 2B). The ponderosa pine LWa width chronology is significantly correlated with spring precipitation totals (both March and April), and the monthly correlations with precipitation during the preceding autumn and winter are mostly not significant (Figure 2B). Therefore, we

https://doi.org/10.15447/sfews.2023v21iss1art2

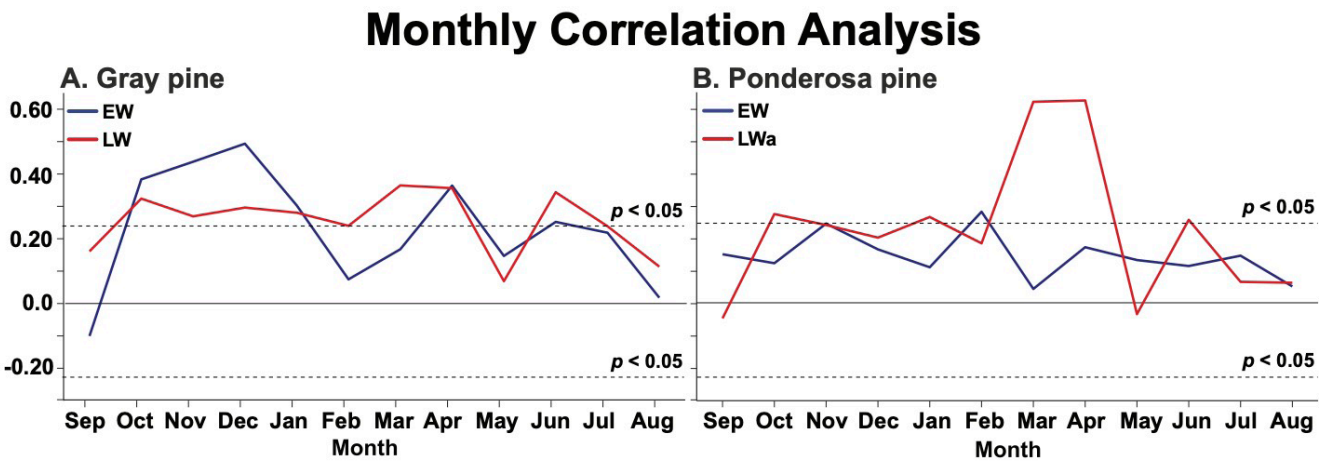

Figure 2 (**A**) The gray pine chronologies of earlywood (EW; *blue*) and latewood width (LW; *red*) are correlated with monthly precipitation totals for the region within the *black box* (Figure 1) from 1948–2017 (coefficients from prior September to August concurrent with tree growth are plotted). Note that the EW chronology is best correlated with precipitation during "autumn" (Oct–Dec). (**B**) Same as (**A**) for the ponderosa pine chronologies of EW and adjusted latewood width (LWa). Note the strong positive correlation between adjusted latewood width and "spring" precipitation (Mar–Apr).

used the LWa width chronology to reconstruct spring precipitation (Mar–Apr).

Seasonal Precipitation Reconstructions

The calibration and verification statistics indicate the sub-annual and annual tree-ring width data can be used to provide preliminary estimates of autumn, winter, and spring precipitation variability over northern California. Only two gray pine EW width chronologies are currently available, but they explain 43% of the interannual variability in the transformed autumn precipitation totals (Oct–Dec) during the 1948 to 2017 calibration period (r = 0.66; $p < 0.0001$; Figure 3A, Table 2). The relationship between reconstructed and instrumental autumn precipitation is weaker when based on the 1983 to 2017 verification period, but the RE and CE statistics both indicate that the reconstruction provides some skill when compared with independent autumn precipitation data (Table 2). The autumn reconstruction only extends back to 1897 but is sufficient to demonstrate potential for tree-ring reconstruction of precipitation during the early wet season in California. The Walker Ridge gray pine chronology dates from 1897 to 2017, but the Finley Lake chronology dates from 1771 to 2018 (Table 1), indicating that longer chronologies for this interesting species should be possible.

Full wet season precipitation totals (Oct–Apr) were reconstructed from four blue oak chronologies of RW. The reconstruction explains 79% of the variability in instrumental wet-season precipitation (r = 0.89, $p < 0.0001$). Experiments with split calibration/verification periods suggest that the relationship between blue oak growth and wet- season precipitation has been stable during the instrumental record from 1900 to 2003 (Table 2, Figure 3B).

We reconstructed spring precipitation totals (Mar–Apr) from the regional ponderosa pine LWa width chronology. The reconstruction explains 56% of the interannual variability of the log-transformed spring precipitation totals during the full calibration period (r = 0.75, $p < 0.0001$; Table 2). Split period calibration and verification tests were performed that indicate adequate calibration and verification of the spring reconstruction (Table 2). The back-transformed spring reconstruction correlates with the instrumental observations for spring from 1948 to 2017 at $r = 0.73$ ($p < 0.0001$; Figure 3C, Table 2). The spring reconstruction also correlates with the instrumental data from 1900 to 1947 (r = 0.61;

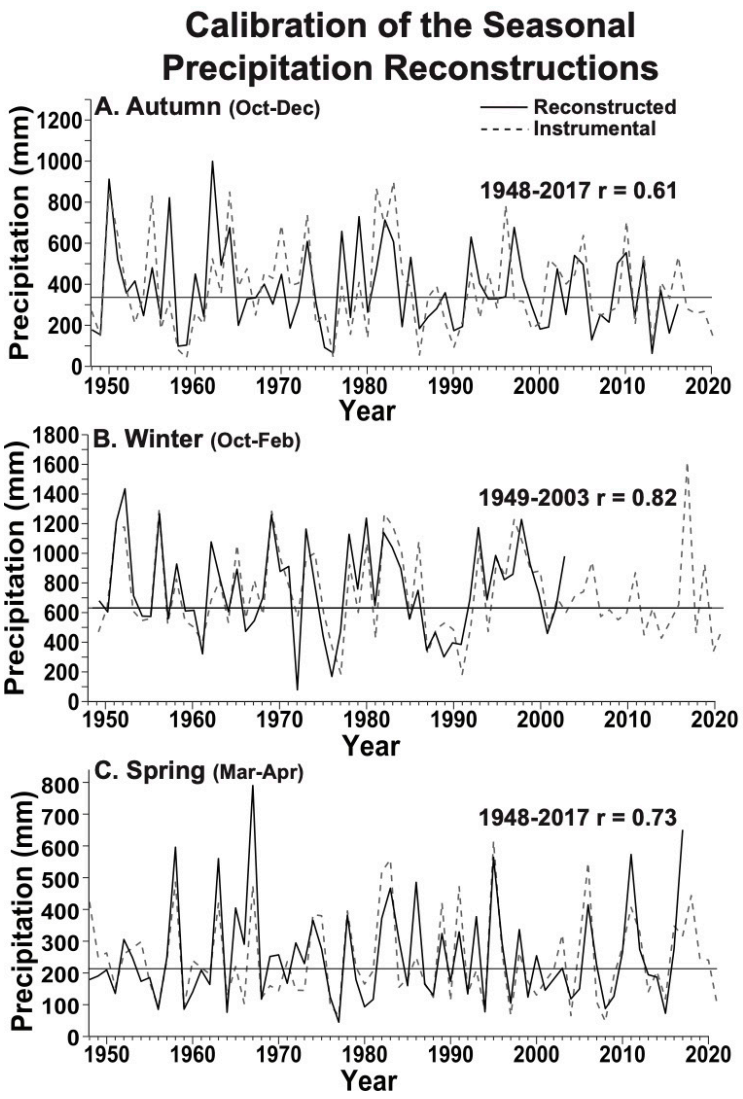

Figure 3 Observed and tree-ring reconstructed precipitation totals are plotted for the (**A**)) autumn (Oct–Dec), (**B**) winter (Oct–Feb), and (**C**) spring (Mar–Apr) seasons during the instrumental era, 1948–2022. Note that the *r*-values shown for autumn (**A**) and spring (**C**) were computed following the back transformation of the reconstructed estimates.

$p < 0.0001$). The spring estimates are based on only two chronologies with relatively low sample sizes (Table 1), but the calibration and verification statistics are promising, and may be improved upon once additional LW width chronologies can be developed in California.

The reconstructions of wet season and spring precipitation make it possible to derive a more narrowly focused estimate of "winter" season precipitation (i.e., Oct–Feb). The winter reconstruction is computed by subtracting reconstructed spring precipitation totals (Mar–Apr) from the full wet season reconstruction. The derived winter reconstruction correlates with the instrumental winter precipitation totals at r = 0.82 from 1949 to 2003 ($p < 0.0001$) and at r = 0.72 ($p < 0.0001$) from 1900 to 1948 (Figure 3B, Table 2).

We correlated the autumn, winter, and spring reconstructions with gridded instrumental precipitation in California for a spatial perspective on the seasonal moisture signal in these tree-ring estimates (Figures 4A–4C; note the overlap of months in autumn and winter). The spatial correlations for the autumn reconstruction are weaker and are spread across most of northern California (Figure 4A). The highest correlations are observed in and near the study area for the winter (Figure 4B) and spring reconstructions (Figure 4C).

https://doi.org/10.15447/sfews.2023v21iss1art2

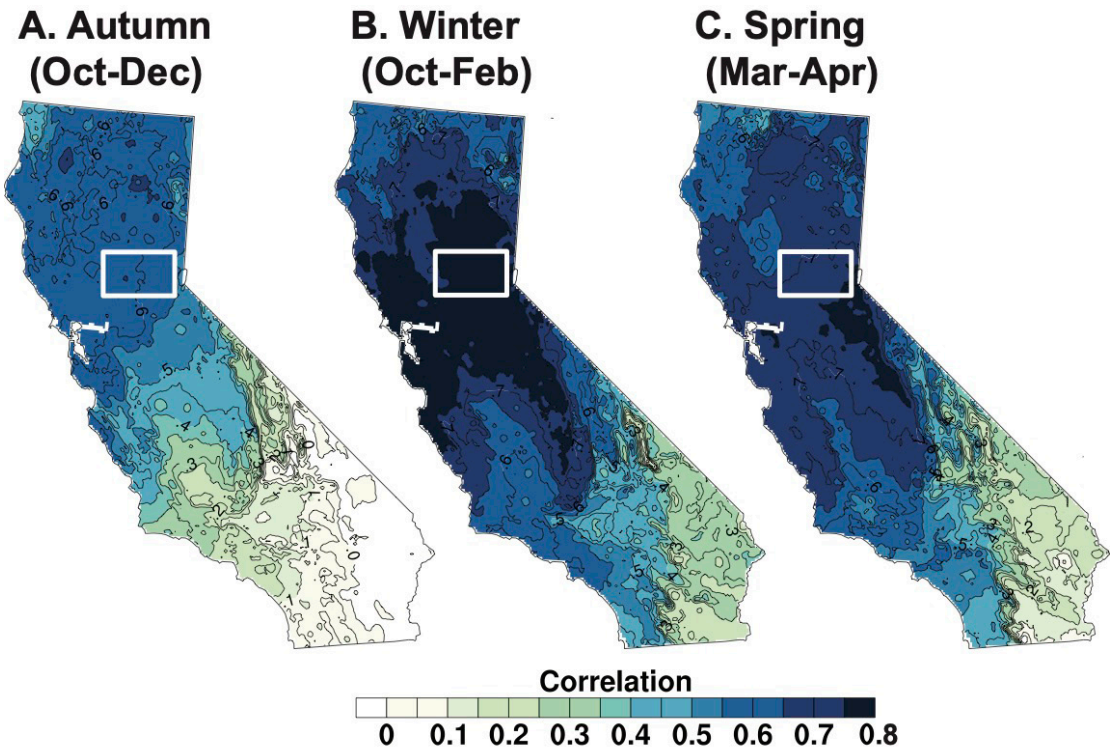

Figure 4 The correlation of the tree-ring reco nstructed seasonal precipitation totals for the northern California study area with gridded seasonal totals statewide [(**A**) autumn (Oct–Dec), (**B**) winter (Oct–Feb), (**C**) spring (Mar–Apr) for the common period 1948–2017]

The instrumental and reconstructed seasonal precipitation series were also correlated with the IVT (Gelaro et al. 2017; Figure 5) to illustrate the connection between ARs and seasonal totals. The instrumental data are correlated with seasonalized IVT over a broad area of the southeast Pacific Ocean and extending into western North America in all three seasons, consistent with the transport of tropical moisture in ARs (Figures 5A–5C). The reconstructed seasonal precipitation totals exhibit the same spatial patterns of correlation with IVT over the Pacific and western North America, but the correlations are lower, especially for autumn (Figures 5D–5F).

The spatial correlations with IVT are at or above $r = 0.80$ for the instrumental and reconstructed winter and spring precipitation totals (Figure 5), indicating that ARs can dominate the interannual variability of seasonal precipitation in central California. These results also provide a useful test for the seasonal reconstructions because they exhibit AR-like patterns of correlation with vapor transport like the instrumental seasonal totals. The time-series of reconstructed seasonal precipitation may therefore provide useful upper and lower limits on the long-term history of landfalling ARs in the study area.

Daily Correlation Analyses of the Seasonal Precipitation Reconstructions

Correlation analysis with daily precipitation data can more precisely specify the climate signal present in the seasonal precipitation reconstructions (e.g., Howard and Stahle 2020). The seasonal reconstructions are correlated with instrumental daily precipitation summed for *n*-consecutive days moving through the water year at 1-day time intervals in Figure 6. The daily correlations for the reconstruction of "autumn" precipitation are highest with 90-day precipitation summed from autumn, but weaker precipitation correlations are also computed in the following spring and summer (Figure 6A). The instrumental autumn precipitation totals share some of this

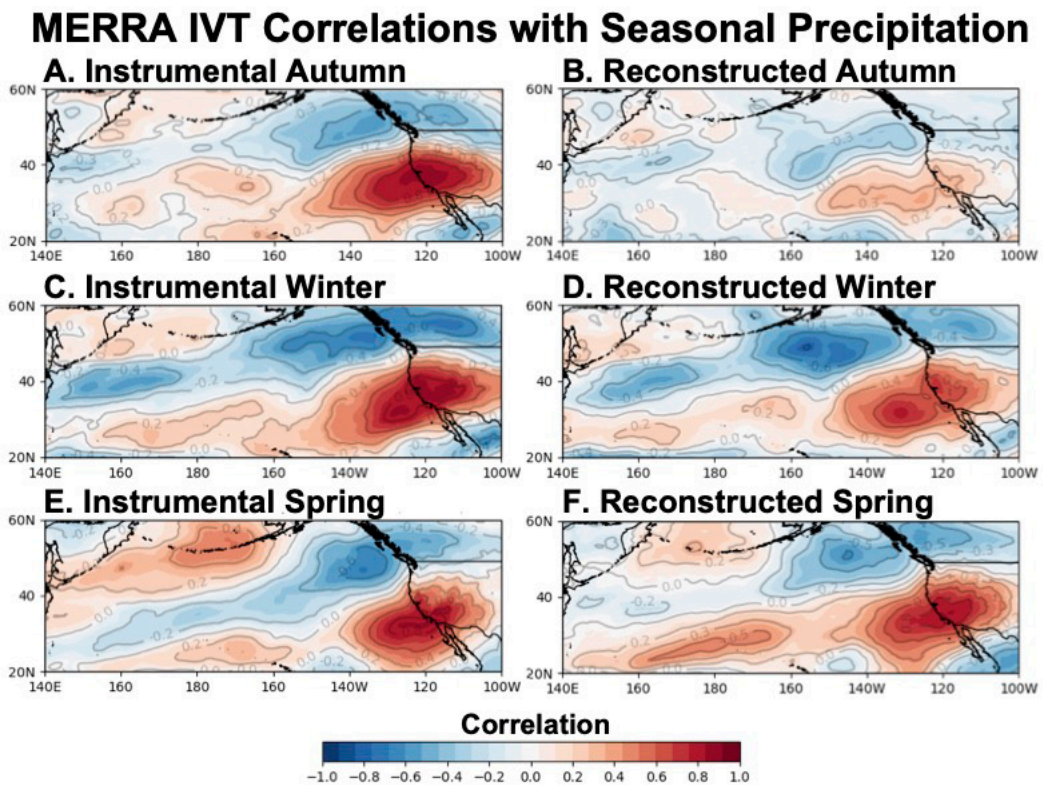

Figure 5 Gridded integrated vapor transport (IVT) data from MERRA-2 (Gelaro et al., 2017) summed for autumn (Oct–Dec; **A**, **B**), winter (Oct–Feb; **C**, **D**) and spring (Mar–Apr; **E**, **F**) were correlated with the respective instrumental and reconstructed seasonal precipitation totals for the study area. The correlations are based on 1980–2003 for winter, and 1980–2017 for autumn and spring.

weak correlation in the subsequent summer (Figure 6A).

The full wet season reconstruction has an integrated precipitation response that faithfully reproduces the response profile of the instrumental wet season precipitation data (blue and black lines in Figure 6B, respectively). However, when the spring signal is removed by subtracting the spring reconstruction from the wet season estimates, the derived winter reconstruction is best correlated with 150-day precipitation from October to March (maximum $r = 0.84$ from October 4 to March 2; red line in Figure 6B). Note the rapid decline in correlation after early March, indicating the winter estimates are largely independent of precipitation totals for the next 2 months. An experimental Jan–Feb ("midwinter") reconstruction is also computed by subtracting autumn and spring from the wet season reconstruction. The resulting time-series is correlated with midwinter precipitation at $r = 0.57$ ($p < 0.0001$) from 1949 to 2003 and 0.43 from 1900 to 1948 (Table 1). These correlations are marginal, but it may eventually be possible to enhance this midwinter precipitation estimate based on blue oak RW chronologies and improved reconstructions of shoulder-season precipitation totals.

The daily correlation profiles for instrumental and reconstructed spring precipitation are similar (red and black lines in Figure 6C). The highest correlation for the spring reconstruction is with 60-day precipitation totaled from February 22 to April 23 for 1948 to 2017 ($r = 0.79$ [$p < 0.0001$]; red line in Figure 6C). The ponderosa pine LW chronology (no adjustments) also positively and significantly correlated with 60-day total precipitation in spring, but the level of correlation is much lower compared to the reconstruction based on the LWa data (blue line in Figure 6C),

https://doi.org/10.15447/sfews.2023v21iss1art2

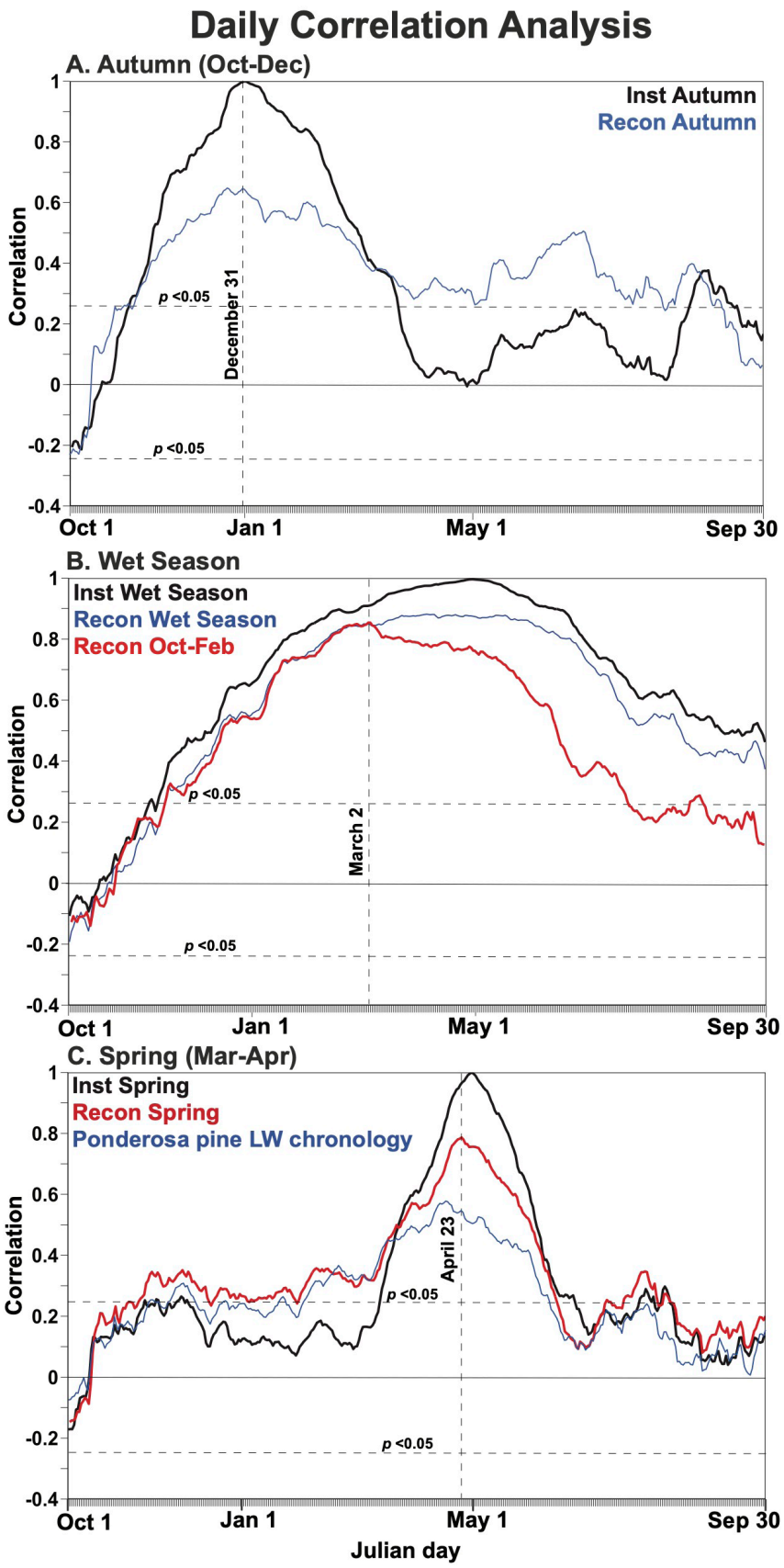

Figure 6 (**A**) The autumn reconstruction (Oct–Dec, *blue curve*) was correlated with daily precipitation totals summed for all possible 90-day intervals advancing one day at a time through the water year. For comparison, the instrumental daily precipitation data summed for 90 days from Oct 3 to Dec 31 were averaged for the study area and then also correlated with all 365 possible 90-day instrumental totals advancing in 1-day intervals through the water year (i.e., instrumental vs instrumental, black curve). (**B**) Same as (**A**) but using the wet season reconstruction (Oct–Apr) from blue oak. The wet season reconstruction was correlated with precipitation totaled for 210 days (*blue curve*), the derived winter (Oct–Feb) precipitation estimates were correlated with precipitation totals for 150 days (*red curve*) for the period 1949-2003, which is in common between the blue oak and instrumental precipitation data. (**C**) Same as (**A**) for the spring reconstruction (Mar–Apr, *red curve*). The ponderosa pine LW chronology (with no adjustment) was also correlated with 60-day precipitation totals (*blue line*). The *vertical dashed lines* represent the day when the highest correlation is reached between each reconstruction and seasonal precipitation variable, and the *horizontal dashed lines* represent the thresholds for significant correlation ($p < 0.05$).

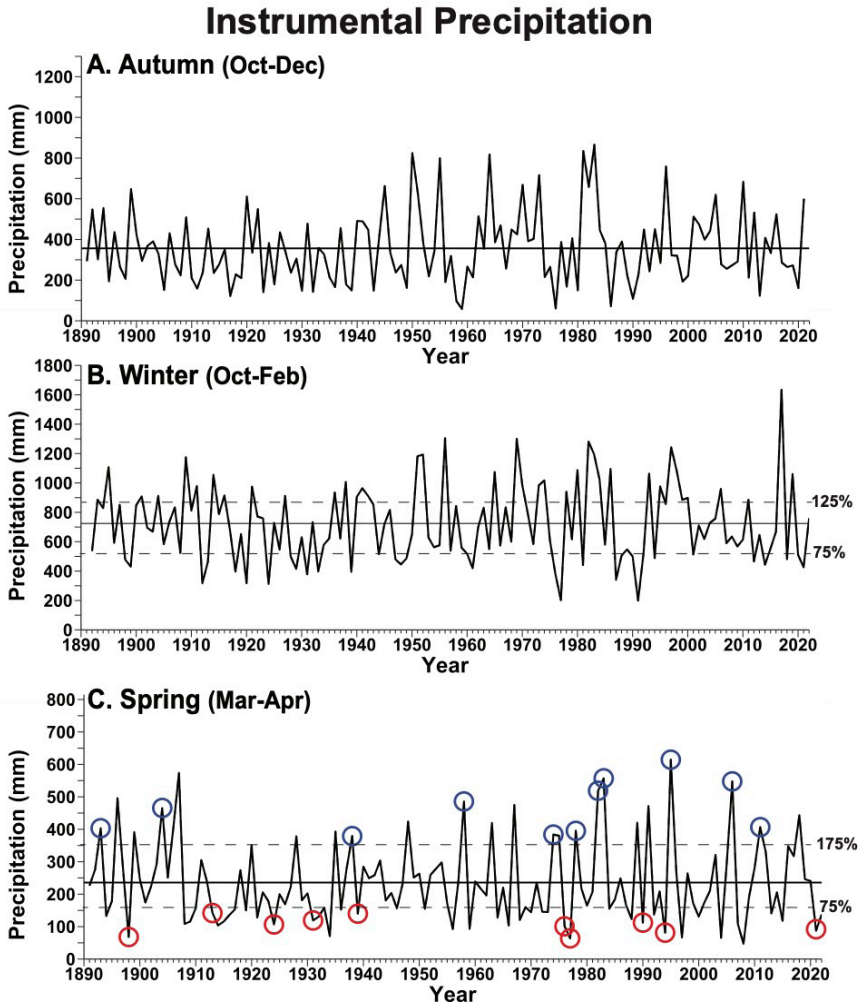

Figure 7 Instrumental precipitation totals are plotted for the three seasons recorded by the tree-ring data from California, including (**A**) autumn (Oct–Dec), (**B**) winter (Oct–Feb), and (**C**) spring (Mar–Apr). The precipitation data from 1891–2016 are from the GPCC product and the CPC data for 2017–2022 are appended for the northern California study area. The median is plotted for each season. (**C**) Years when instrumental spring precipitation was very wet (≥ 175% of median or greater) following a wet winter (i.e. ≥ 125% of median or greater) are indicated with *blue circles*, and years when both seasons were less than or equal to 75% of their respective medians are indicated with *red circles.* The *dashed lines* in (**B**) and (**C**) represent the 125 and 175% of median values for winter and spring, respectively.

highlighting the value of signal enhancement in these sub-annual ring width data.

Analysis of Instrumental and Reconstructed Seasonal Precipitation

These results indicate the potential to use sub-annual chronologies of EW and LW width to estimate shoulder-season precipitation over the past 270 years, in addition to the reconstructions of wet-season or water-year totals already possible with RW chronologies. The instrumental record of seasonal precipitation is plotted for the study area from 1891 to 2022 using the "seasons" most strongly associated with the available tree ring data (Oct–Dec, Oct–Feb, and Mar–Apr; Figure 7; note that the CPC observations are appended to these GPCC seasonal time-series for 2017 to 2022). The frequency of high precipitation totals has varied for all three seasons (Figure 7), but no significant linear trends are detected in the mean or variance of the instrumental seasonal precipitation totals over the full period of 1891 to 2022. (We evaluated variance trend by computing the residuals above or below the median for each

https://doi.org/10.15447/sfews.2023v21iss1art2

season, and testing the significance of the slope of a regression line fit to the absolute values of the residuals.) If the investigation of the spring precipitation trend were restricted to the period from 1910 to 2022, the increase in variance would be significant ($p < 0.01$; Figure 7C).

The decadal variability of hydroclimate in California has been documented (Florsheim and Dettinger 2007; Ault and St. George 2010; St. George and Ault 2011; Dettinger and Cayan 2014), and there appears to be variance modulation of the seasonal totals on decadal time-scales (Liu et al. 2018; Figures 7 and 8). Low variance in spring (Mar–Apr) precipitation was observed during the relatively dry decades of the early 20th century (Figure 7C), and before 1940 in the autumn totals (Oct–Dec; Figure 7A), but there is no strong evidence for a drying trend in the study area for these particular shoulder seasons as detected elsewhere in California (e.g., Swain et al. 2018; Goss et al. 2020; Luković et al. 2021).

The tree-ring reconstructions for autumn (Oct–Dec), winter (Oct–Feb), and spring precipitation (Mar–Apr) are plotted in Figure 8. Autumn precipitation in the study area was enhanced during the mid 20th century in both the instrumental and reconstructed series (Figures 7A and 8A). Strong decadal to multi-decadal variability is evident in the winter reconstruction (Figure 8B) and is also apparent in the instrumental data during the relatively dry 1920 to 1930s and wet 1960s to 1970s (Figure 7B). Major winter wet episodes are reconstructed for the 1820s to 1830s and the 1860s to 1870s (Figure 8B), including 1862 and 1868, which were among the five wettest years in the entire reconstruction and were among the wettest years in the weather history of California (Kelly 1989; Stahle et al. 2013).

Reconstructed spring precipitation was subject to episodes of relatively frequent and infrequent wet extremes in the pre-instrumental period (e.g., 1801 to 1850 vs. 1851 to 1900 for estimates ≥175% of median; Figure 8C). Episodes of wet extremes are also evident in the instrumental observations of spring precipitation (Figure 7C). Spring precipitation only represents some 24% of the median wet-season totals in the instrumental record (22% in the reconstructions), but anomalously low or high precipitation in spring can certainly translate into significant effects on stream and water supply in California.

Winter and Spring Precipitation Anomalies

The relevance of spring precipitation anomalies to flood risk and water supply in northern California can be illustrated with accumulated regional precipitation and stream discharge in the American River at Folsom. (The study area is largely co-located with the drainage basin of the America River, and these instrumental wet-season precipitation and discharge data are correlated at $r = 0.94$.) Daily precipitation totals in the study area are cumulated from October 1 to July 15 for just those years when spring precipitation (Mar–Apr) was in the upper 80th or lower 20th percentile (15 years each) and are plotted along with the accumulated mean of all 74 years from 1949 to 2022 (Figure 9A). Accumulated precipitation in wet springs averaged 1,267 mm on April 30 compared with the average of 984 mm for all years (1949 to 2022) and with 706 mm for the 15 anomalously dry springs (Figure 9A). These represent percentage differences from the 74-year average precipitation on April 30 of 29% above average for the wet springs and 28% below average for the dry springs.

Cumulative monthly mean discharge averaged 2.5 million acre-feet (af) on April 30 during the wet springs, compared with the 74-year average of 1.85 million af (1949 to 2022) and with 1.2 million af for the 15 anomalously dry springs (both 35% above or below the 74-year average; Figure 9B; similar differences were observed at the end of the snowmelt season). These differences in precipitation and discharge are primarily the result of the anomalously wet or dry spring conditions, but antecedent anomalies in winter also contributed, especially for the precipitation data (Figures 9A and 9B). Cumulative precipitation and discharge for the remaining 44 years that did not record wet or dry spring precipitation totals are plotted for comparison in Figures 9C and 9D. Note that spring precipitation

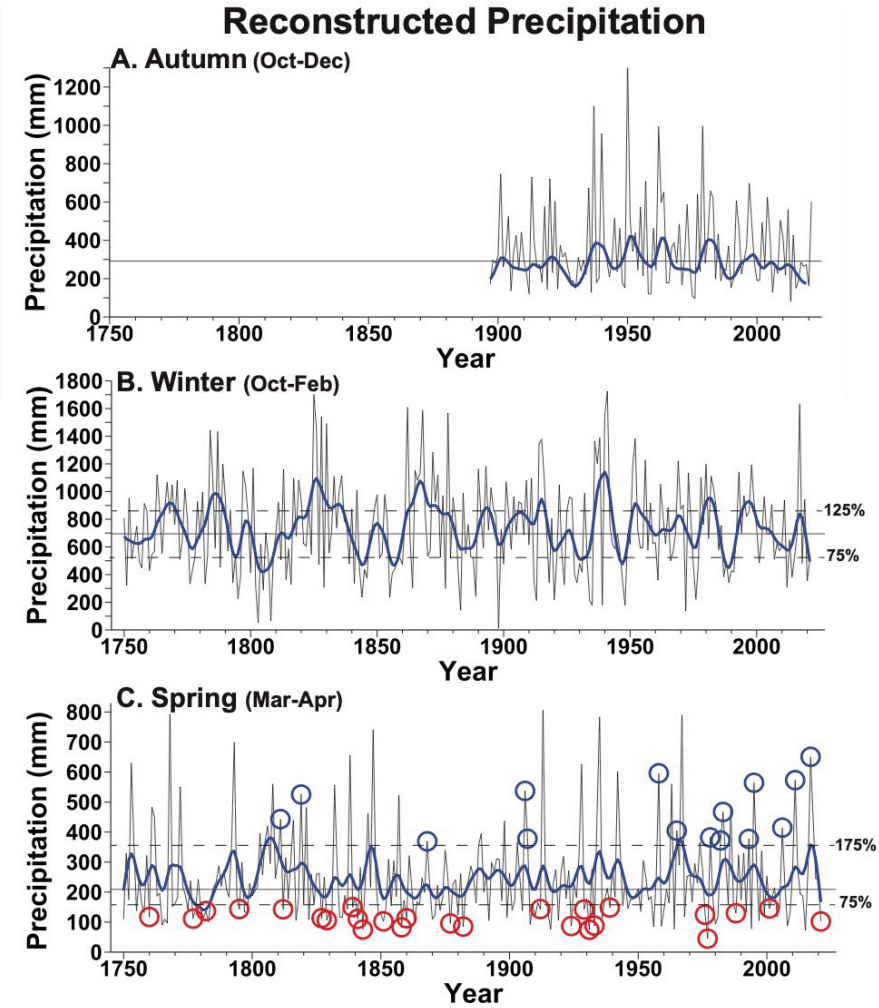

Figure 8 (**A**) The autumn (Oct–Dec) precipitation reconstruction is plotted from 1897–2021. The (**B**) winter (Oct–Feb) and (**C**) spring (Mar–Apr) precipitation reconstructions are plotted from 1750–2022. Instrumental observations have been appended after 2017 (**A**, **C**) and 2003 (**B**). (**C**) Years when instrumental spring precipitation was very wet (≥175% of median) following a wet winter (≥125% of median) are indicated with *blue circles*, and years when both winter and spring precipitation were ≤75% of median are indicated with *red circles* (computed for the interval in common to both reconstructions, 1750–2003). The reconstructions are fit with 10-year smoothing splines to emphasize decadal variability (*blue curves*; *Cook and Peters 1981*). The *dashed lines* in (**B**) and (**C**) represent the 125 and 175% of median values for winter and Mar–spring, respectively.

was in the 80th percentile for three of the four wettest accumulated wet-season totals (Oct–Apr; Figure 9A), and spring was also very wet in 2017 (i.e., 75th percentile)–the wettest year in the study area from 1949 to 2022 (Figure 9C).

Cumulative precipitation is well separated for most individual years during these wet or dry springs (Figure 9A). The spring precipitation anomalies continued pre-existing moisture regimes established during the antecedent winter months, particularly during wet years (Figure 9A). This tendency for wet springs to follow wet winters (defined here and below as ≥175% of median for spring and ≥125% for winter) is significant in a contingency table analysis of the instrumental precipitation data from 1892 to 2022 (i.e., we observed 11 wet springs following wet winters, compared to our expectation of only seven cases, $p < 0.05$). Wet springs have a lower-than-expected occurrence following a wet winter in the reconstructions from 1750 to 1891($p < 0.05$), but only 3 years were in the wet spring category (i.e., ≥175%) and only 6 wet springs were

https://doi.org/10.15447/sfews.2023v21iss1art2

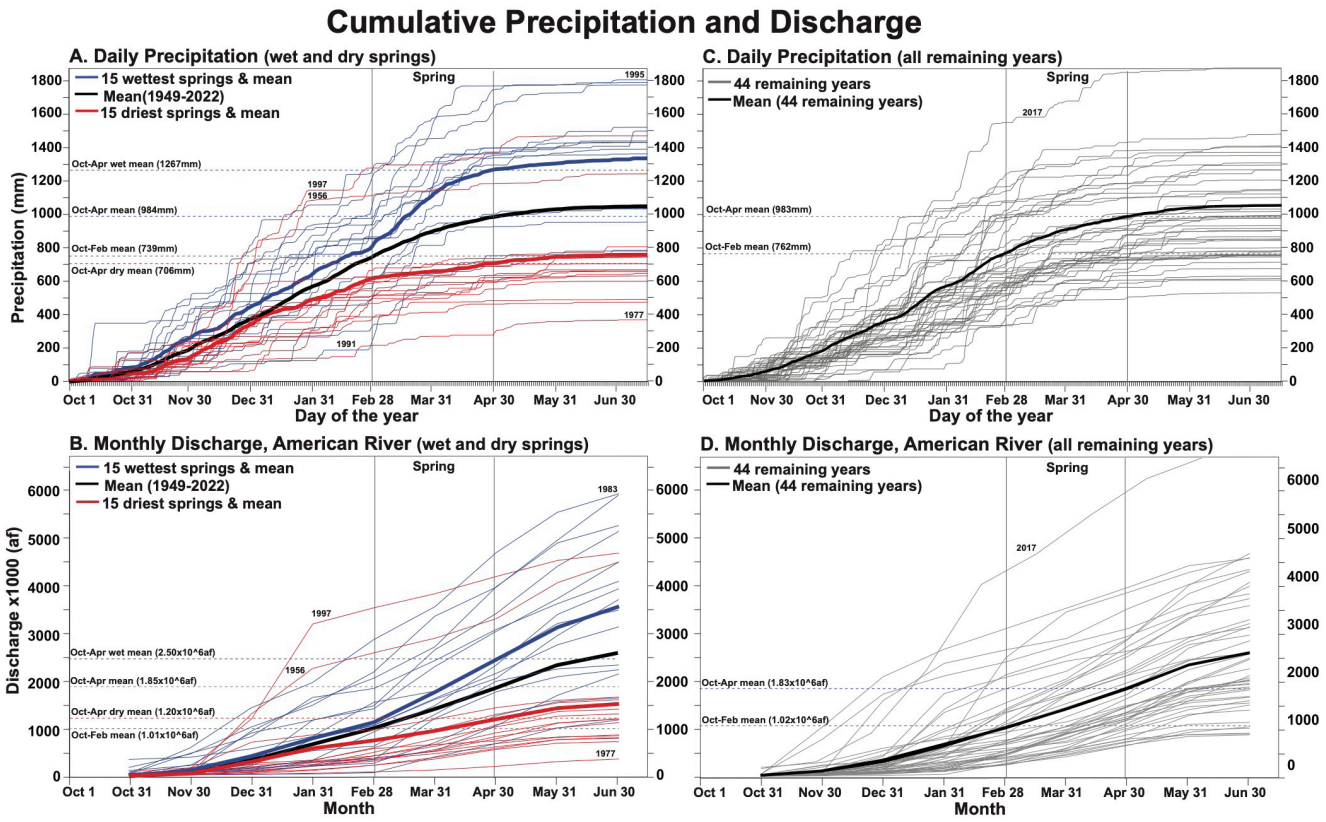

Figure 9 (**A**) Daily precipitation totals in the northern California study area are accumulated from Oct 1 to Jul 15 for spring precipitation anomalies in the upper and lower 20th percentiles of all springs (wet in *blue* and dry in *red*, 15 years each), along with the cumulative daily average precipitation for all 74 years (*black*; 1949–2022). The spring season (Mar 1–Apr 30) is indicated by the *vertical lines*, along with the cumulative average precipitation for Oct–Feb and Oct–Apr. The cumulative averages on Apr 30 are also plotted for the wet and dry spring cases and a few single year extremes are labeled. (**B**) Same as (**A**), but monthly mean streamflow in the American River at Folsom is accumulated for each month from Oct-Jun for the same years when spring precipitation was in the upper or lower 20th percentiles. The cumulative monthly mean discharge is plotted in *black*. (**C**, **D**) Same as (**A**, **B**) for the years from 1949–2022 that did not register an anomalously wet or dry spring (means computed in **C** and **D** for just these 44 years). The monthly streamflow data were acquired from the California Department of Water Resources.

expected. There were also interesting reversals in the precipitation regime from winter to spring (e.g., 1997 vs. 1991; Figure 9A). The "Miracle March" of 1991 was a major reversal when a very dry winter was followed by significant precipitation during spring that brought the cumulative precipitation totals into the near-normal range by April 30 (Figure 9A).

The average increase in precipitation and discharge from the end of winter (March 1) to the end of spring (defined here as April 30) was naturally also affected by anomalous spring precipitation amounts. On average, cumulative precipitation normally increases 33% from March 1 to April 30 in the study area (739 to 984 mm, Figure 9A), but for the 15 wettest springs it increased 59% (796 to 1,267 mm), or 26% above the average increase. In the 15 driest springs, precipitation increased from March 1 to April 30 by only 15% (613 to 06 mm), or 18% below average. Average accumulated discharge typically increases by 85% from March 1 to April 30 (1.0 to 1.85 million af), but the increase was 112% during the wet springs (1.18 to 2.5 million af) or 27% above average (reflecting again both wetter winter and especially wetter spring conditions). In dry spring conditions, the increase in discharge was only 27% of average (0.76 to 1.2 million af, a 58% increase, 27% below average). In these analyses,

anomalously wet (or dry) spring precipitation totals occur in only 1 out of every 5 years, but they have long represented targets of opportunity for water-resource management.

The tree-ring reconstructions of seasonal precipitation totals reproduce the changes in wet and dry springs recorded by the instrumental observations. During the anomalously wet springs (80th percentile), precipitation increased from March 1 to April 30 approximately 20% to 30% above the average increase from the end of winter (Oct–Feb) to the end of spring (Mar–Apr) in both the instrumental and reconstructed data (using common intervals of 1900 to 2003 and 1949 to 2003). However, during the relatively wet interval in reconstructed spring precipitation from 1801 to 1850 (Figure 8C), the increase from the end of winter to the end of spring was 82% for the wet spring anomalies (≥80th percentile; 10 cases), or 49% above the average increase. During the comparatively dry interval from 1851 to 1900, the reconstructed spring increase was also above average (52 vs. 33%), but only by 19%. These comparisons using the tree-ring reconstructions illustrate natural multi-decadal variations in March and April's contributions to the wet season total before the modern record. Skillful tree-ring reconstructions of seasonal precipitation totals for winter and separately for spring can therefore provide a useful pre-instrumental perspective relevant to both natural variability and anthropogenic climate change at this critical seasonal juncture in the water year.

Inspecting the transition from winter to spring in the instrumental and reconstructed precipitation data, the frequency of a wet spring following a wet winter appears to have increased since the mid 20th century (Figures 7 and 8). The years when a wet spring followed a wet winter are highlighted on the spring instrumental (1891 to 2022) and reconstructed precipitation data (1750 to 2022) in Figures 7C and 8C. For an initial assessment, wet-on-wet precipitation anomalies are defined simply as years when the winter total was ≥125% of median and the subsequent spring total was ≥175% of median, corresponding to a wet season precipitation total of approximately 1,234 mm (or 135% of the wet-season median).

There were 44 wet winters in the instrumental data from 1892 to 2022 (i.e., 34% of all 131 years of recorded winter precipitation was ≥125% of median). In those 44 wet winters, the subsequent spring was very wet in 11 of the same years (≥175% of median; 8.4% of all 131 years), but the frequency of these wet-on-wet anomalies does not appear to have been stationary through time. Before and after 1956, the likelihood changed from 4.6% to 12.1% (3 of 65 vs. 8 of 66 years). When evaluated on March 1 after winter precipitation was already known to have equaled or exceeded 125% of median, the probability for a very wet spring went from 15% to 33% before and after 1956 in the instrumental observations (3 of 20 vs. 8 of 24 years; Figure 7C). Similar changes are evident in the tree-ring reconstructions of winter and spring precipitation before and after 1956 (Figure 8C). These changes in winter and spring wetness were not simply the result of the increased amplitude of seasonal precipitation totals during the mid- to late-20th century. Reconstructed winter and spring precipitation extremes have varied on multi-decadal time-scales since 1750 (Figure 8B and 8C), and in the instrumental observations since 1892 (Figures 7B and 7C). Instead, the co-occurrence of wet winters with very wet spring conditions appears to have increased after the mid-1950s. Note that the increased frequency of wet-on-wet conditions is also observed when the tree-ring chronologies are calibrated with the instrumental seasonal precipitation totals in both the early- and late-20th century.

The frequency of low winter and low spring precipitation, when both seasons were ≤75% of median, has also been subject to multi-decadal variability (Figures 7C and 8C). However, dry-on-dry events account for only 8% and 10% of all years in the instrumental and reconstructed data, respectively. The reconstructed dry-on-dry episodes appear to have clustered during the mid 19th and early 20th centuries during extended winter drought episodes (comparing Figure 8B and 8C).

https://doi.org/10.15447/sfews.2023v21iss1art2

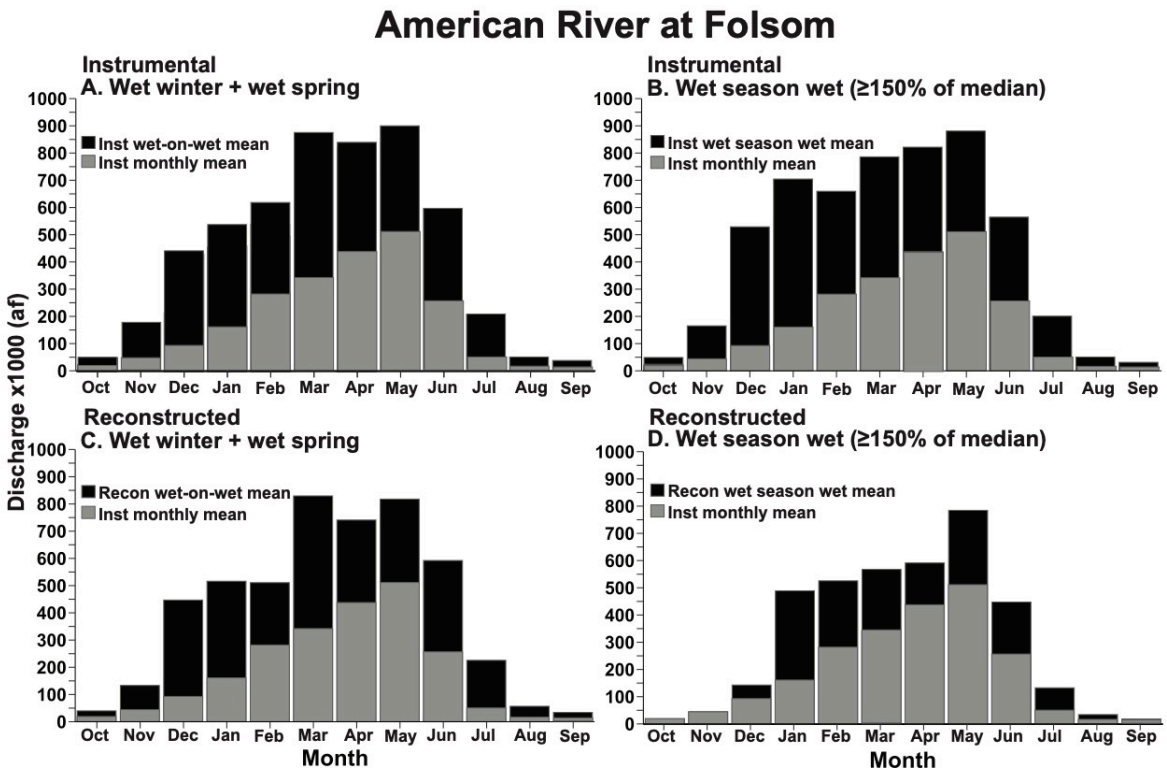

Figure 10 (**A**) Mean monthly streamflow for each month of the water year is calculated using the 10 wet-on-wet years identified using the instrumental precipitation data for the common period 1901–2022 (*black bars*). The long-term monthly means are also plotted for comparison (*gray bars*). (**B**) Mean monthly streamflow for the 12 years from 1901–2022 when wet season (Oct–Apr) total precipitation was ≥150% of median (*black bars*) is compared with the long-term monthly means (*gray bars*). (**C**) Same as (**A**) but using the nine wet-on-wet years identified with the reconstructed precipitation data from 1901–2003. (**D**) Same as (**B**), but for the 12 years when reconstructed wet season precipitation was ≥150% of median.

Above-average winter and spring precipitation in the study area is associated with augmented streamflow and elevated flood risk in the American River, whether based on the instrumental (Figure 10A) or tree-ring-reconstructed seasonal precipitation totals (Figure 10C). Monthly streamflow is considerably enhanced when a wet spring follows a wet winter, especially from March to June for both the instrumental and reconstructed wet-on-wet years (Figure 10A and 10C). The highest monthly streamflow typically occurs in May as a result of snowmelt from the Sierra Nevada in the American River basin, but, during years when very wet springs follow wet winters, the monthly streamflow surge tends to begin in March (Figure 10A and 10C).

Streamflow data for years when the total wet season precipitation anomaly was ≥150% of median (1,384 mm) are also plotted for comparison with the averages during the wet-on-wet winter–spring conditions (Figure 10B and 10D). Monthly streamflow is above normal for all months in these wet years, peaking in May (Figure 10B), and these results are similar if a higher precipitation threshold is used (e.g., ≥200% of median, not shown). However, streamflow averages for the wet-on-wet winter–spring years are even higher compared to just the wet season extremes, especially during March and April (Figure 10).

Spring streamflow (here defined as Mar–May) for the American River at Folsom is plotted from 1901 to 2022 to illustrate the connection between wet-on-wet winter and spring precipitation extremes and elevated Mar–May runoff (Figure 11). Wet-on-wet winter and spring precipitation extremes produced some of the highest spring stream

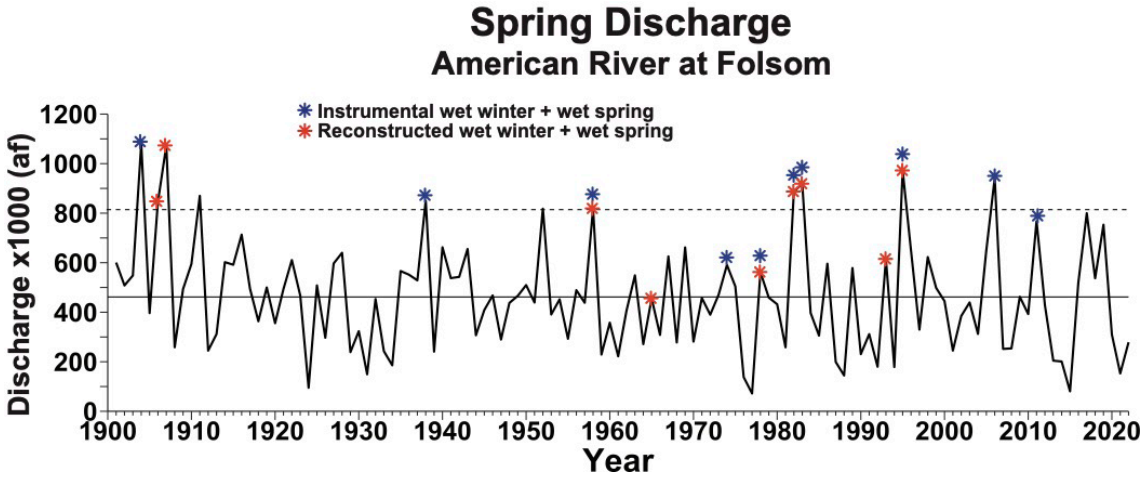

Figure 11 Spring streamflow is plotted for the American River at Folsom from 1901–2022 (Spring is March through May average streamflow). Instrumental (*blue symbols*) and reconstructed (*red symbols*) years of wet winter and very wet spring precipitation totals are noted to emphasize the connection between wet-on-wet years and elevated spring streamflow. The *dashed line* corresponds to 803,000 cfs, or approximately the 90th percentile of March though May streamflow.

levels for the American River at Folsom since 1901 (Figure 11). The years with wet winter and very wet spring precipitation totals in the instrumental and reconstructed series occurred during six of the ten highest spring streamflow averages recorded on the American River. Reconstructed winter and spring precipitation were both above median in 3 of the 4 remaining years. These results provide additional credibility for the seasonal reconstructions even though the sample size is low.

DISCUSSION AND CONCLUSIONS

These results demonstrate that annual and sub-annual ring width chronologies of gray pine, ponderosa pine, and blue oak can vary proportionally with discrete seasonal precipitation totals in California, and may therefore provide insight into seasonal climate variability and change. Gray pine has not to our knowledge been used for dendroclimatic reconstructions, but the fall precipitation signal of gray pine EW width could have important applications to seasonal precipitation analysis in California. The literature concerning gray pine phenology is limited, but Launchbaugh et al. (1956) noted that growth for this lower-elevation species can begin in autumn with the first rains of the wet season and continue into the following spring and summer. Powers (1990) also noted that gray pine photosynthesis can take place during the cool season. Some of the EW component of the annual ring in gray pine may therefore be formed concurrently with autumn precipitation in the year before the spring–summer growing season, when the annual rings of most trees in California are formed.

Winter and spring precipitation totals are not significantly correlated in the instrumental or reconstructed data, but the occasional co-occurrence of winter and spring anomalies can be very consequential in terms of flood risk and water supply. Some elevated streamflow events associated with wet-on-wet winter and spring conditions resulted in severe flooding, notably in 1907, 1958, 1982, 1983, and 1995. The spring flooding for these years can be traced back to intense storms late in the wet season that delivered precipitation to already saturated landscapes and swollen streams (USGS 1958). A very wet spring following an already wet winter occurred just 11 times in the instrumental observations from 1892 to 2022, but most of these co-occurring wet anomalies were observed during the late 20th century in both the instrumental and reconstructed time-series. A dry winter followed

https://doi.org/10.15447/sfews.2023v21iss1art2

by a dry spring can significantly reduce water supply and these co-occurring seasonal droughts appear to have clustered during multi-decadal episodes of reconstructed winter dryness during the mid-19th and early-20th century.

The precipitation and flooding extremes of 1862 are famous in the weather and runoff history of California (Kelly 1989). Previous tree-ring reconstructions of 1862 based on RW chronologies are well above average, but the reconstructed value for 1862 was eclipsed by estimates for 1868 and several other very wet years in both northern and southern California (e.g., Stahle et al. 2013). Documentary accounts indicate that the heaviest precipitation in 1862 fell in January and February, and the spring totals were only average to below average over parts of California (Cary Mock, 2019 personal communication with DS, unreferenced, see "Notes"). By subtracting the newly reconstructed spring amount for 1862 from the wet season total, the tree-ring estimated precipitation for just "winter" (Oct–Feb) in 1861–1862 is near record, only exceeded by 1941 and 1825 in the reconstruction, and by 2017 in the instrumental portion of the reconstruction (after 2003; Figure 8B). The discrete seasonal response of sub-annual ring width chronologies may therefore lead to improved reconstruction of extreme precipitation amounts in California history.

These results demonstrate the feasibility of seasonal and storm-level precipitation reconstructions in California using a combination of annual and sub-annual tree-ring data. The reconstructions provide an otherwise unavailable centennial perspective on the seasonal precipitation variability relevant to reservoir operations in early spring, when management strategies often shift from flood control to water-resource capture. Because heavy storms associated with landfalling ARs dictate so much of the variability in seasonal to full-wet-season precipitation totals in California, it may be possible to use selected tree-ring data to reconstruct storm-delivered precipitation on a seasonal to annual basis. Improved seasonal reconstructions could also help place the last half-century of shoulder-season precipitation variability—and the co-occurrence of winter and spring precipitation anomalies—into a longer context before the era of increasing anthropogenic influence on California climate and water supply.

ACKNOWLEDGEMENTS

The California Department of Water Resources and University of California San Diego supported this research (Grant No. 003794-00001A). We thank the US Department of Agriculture Forest Service and the California State Parks for permission to conduct this research. We are also grateful for the insightful suggestions and contributions from Mike Dettinger, Marty Ralph, and three anonymous reviewers. Upon publication, the data developed for this article will be available from the authors and will be contributed to the International Tree-Ring Data Bank at the NOAA Paleoclimatology Program (*https://www.ncei.noaa.gov/products/paleoclimatology*).

REFERENCES

Ault TR, St. George S. 2010. The magnitude of decadal and multidecadal variability in North American precipitation. J Clim. [accessed 2021 Aug 1];23:842–850. *https://doi.org/10.1175/2009JCLI3013.1*

Bales RC, Molotch NP, Painter TH, Dettinger MD, Rice R, Dozier J. 2006. Mountain hydrology of the western United States. Water Resour Res. [accessed 2021 Aug 1];42. *https://doi.org/10.1029/2005WR004387*

Belmecheri S, Babst F, Wahl ER, Stahle DW, Trouet V. 2016. Multi-century evaluation of Sierra Nevada snowpack. Nat Clim Chang. [accessed 2021 Aug 1];6;2–3. *https://doi.org/10.1038/nclimate2809*

Box GP, Cox DR. 1964. An analysis of transformations. J R Stat Soc. 26:211–252.

Borkotoky SS, Williams AP, Cook ER, Steinschneider S. 2021. Reconstructing extreme precipitation in the Sacramento River watershed using tree-ring-based proxies of cold-season precipitation. Water Resour Res. [accessed 2021 Aug 1];57:e2020WR028824. *https://doi.org/10.1029/2020WR028824*

Carlón–Allende TJ, Villaneuva–Diaz J, Mendoza ME, Pérez–Salicrup DR. 2018. Climatic signal in earlywood and latewood in conifer forests in the Monarch Butterfly Biosphere Reserve, Mexico. Tree-Ring Res. [accessed 2021 Aug 1];74:63–75. *https://doi.org/10.3959/1536-1098-74.1.63*

Cayan DR, Roads JO. 1984. Local relationships between United States West Coast precipitation and monthly mean circulation parameters. Mon Weather Rev. [accessed 2021 Aug 1];112:1276–1282. *https://doi.org/10.1175/1520-0493(1984)112< 1276:LRBUSW>2.0.CO;2*

Cook ER, Peters K. 1981. The smoothing spline: a new approach to standardizing forest interior tree-ring width series for dendroclimatic studies. Tree-Ring Bull. 41:45–53.

Cook ER. 1985. A time series analysis approach to tree ring standardization [dissertation]. [Tucson (AZ)]: University of Arizona School of Natural Resources. 183 p.

Cook ER, Kairiukstis LA. 1990. Methods of dendrochronology: applications in the environmental sciences. [accessed 2021 Aug 1]. *https://doi.org/10.2307/1551446*

Cook ER, Meko DM, Stahle DW, Cleaveland MK. 1999. Drought reconstructions for the continental United States. J Clim. [accessed 2021 Aug 1];12:1145–1163. *https://doi.org/10.1175/1520-0442(1999)012< 1145:drftcu>2.0.co;2*

Daly C, Neilson RP, Phillips DL. 1994. A statistical-topographic model for mapping climatological precipitation over mountainous terrain. J Appl Meteorol Climatol. [accessed 2021 Aug 1];33:140–158. *https://doi.org/10.1175/1520-0450(1994)033< 0140:ASTMFM>2.0.CO;2*

Dettinger M, Cayan DR. 1995. Large-scale atmospheric forcing of recent trends towards early snowmelt runoff in California. J Clim. [accessed 2021 Aug 1];8:606–623. *https://doi.org/10.1175/1520-0442(1995)008< 0606:LSAFOR>2.0.CO;2*

Dettinger M, Cayan DR. 2014. Drought and the California Delta—a matter of extremes. San Franc Estuary Watershed Sci. [accessed 2021 Aug 1];12(2). *https://doi.org/10.15447/sfews.2014v12iss2art4*

Dettinger MD. 2016. Historical and future relations between large storms and droughts in California. San Franc Estuary Watershed Sci. [accessed 2021 Aug 1];14(2). *https://doi.org/10.15447/sfews.2016v14iss2art1*

Douglass, AE. 1909. Weather cycles in the growth of big trees. Mon Weather Rev. June, 225–237.

Finley K, Zhang J. 2019. Climate effect on Ponderosa Pine radial growth varies with tree density and shrub removal. Forests. [accessed 2022 May 21];10. *https://doi.org/10.3390/f10060477*

Florsheim JL, Dettinger MD. 2007. Climate and floods still govern California levee breaks. Geophys Res Lett. [accessed 2021 Aug 1];34. *https://doi.org/10.1029/2007GL031702*

Gelaro R, McCarty W, Suárez MJ, Todling R, Molod A, Takacs L, Randles CA, Darmenov A, Bosilovich MG, Reichle R, et al. 2017. The modern-era retrospective analysis for research and applications, version 2 (MERRA-2). J Clim. [accessed 2021 Aug 1];30:5419–5454. *https://doi.org/10.1175/JCLI-D-16-0758.1*

Goss M, Swain DL, Abatzoglou JT, Sarhadi A, Kolden CA, Williams AP, Diffenbaugh NS. 2020. Climate change is increasing the likelihood of extreme autumn wildfire conditions across California. Environ Res Lett. [accessed 2021 Aug 1];15. *https://doi.org/10.1088/1748-9326/ab83a7*

Granger O. 1979. Increasing variability in California precipitation. Ann Assoc Am Geogr. [accessed 2021 Aug 1];69:533–543. *https://doi.org/10.1111/j.1467-8306.1979.tb01280.x*

Griffin D, Woodhouse CA, Meko DM, Stahle DW, Faulstich HL, Carrillo C, Touchan R, Castro CL, Leavitt SW. 2013. North American monsoon precipitation reconstructed from tree-ring latewood. Geophys Res Lett. [accessed 2021 Aug 1];40:954–958. *https://doi.org/10.1002/grl.50184*

Griffin D, Anchukaitis KJ. 2014. How unusual is the 2012–2014 California drought? Geophys Res Lett [accessed 2021 Aug 1];41:9017–9023. *https://doi.org/10.1002/2014GL062433*

Higgins R, Shi W, Yarosh E, Joyce R. 2000. Improved United States precipitation quality control system and analysis. NOAA Natl Weather Serv Natl Centers Environ Predict Clim Predict Cent.

Higgins R, Silva S, Shi W, Larson J. 2007. Relationships between climate variability and fluctuations in daily precipitation over the United States. J Clim. [accessed 2021 Aug 1];20:3561–3579. *https://doi.org/10.1175/JCLI4196.1*

Howard CD. 1999. Death to rule curves. In: WRPMD'99: Preparing for the 21st century. 29th Annual Water Resources Planning and Management Conference. American Society of Civil Engineers. [accessed 2022 May 31]. p. 1–5. Available from: *https://ascelibrary.org/doi/10.1061/40430%281999%29232*

Howard IM, Stahle DW. 2020. Tree-ring reconstruction of single-day precipitation totals over Eastern Colorado. Mon Weather Rev. [accessed 2021 Aug 1];148:597–612. *https://doi.org/10.1175/MWR-D-19-0114.1*

Jevšenak J. 2019. Daily climate data reveal stronger climate-growth relationships for an extended European tree-ring network. Quat Sci Rev. [accessed 2021 Aug 1];221. *https://doi.org/10.1016/j.quascirev.2019.105868*

Johnson C, Chhin S, Zhang J. 2017. Effects of climate on competitive dynamics in mixed conifer forests of the Sierra Nevada. For Ecol Manag. [accessed 2022 May 31];394. *https://doi.org/10.1016/j.foreco.2017.03.017*

Kelly RL. 1989. Battling the inland sea: floods, public policy, and the Sacramento Valley. Berkeley (CA): University of California Press. 395 p.

Lamjiri MA, Dettinger MD, Ralph FM, Oakley NS, Rutz JJ. 2018. Hourly analyses of the large storms and atmospheric rivers that provide most of California's precipitation in only 10 to 100 hours per year. San Franc Estuary Watershed Sci. [accessed 2021 Aug 1];16(4). *https://doi.org/10.15447/sfews.2018v16iss4art1*

Launchbaugh JL, Biswell HH, Schultz AM. 1956. The control of Digger Pine with herbicides placed in basal cuts. J Range Manag. [accessed 2022 May 31];11:14–18. *https://doi.org/10.2307/3894670*

Liu YC, Di P, Chen SH, DaMassa J. 2018. Relationships of rainy season precipitation and temperature to climate indices in California: long-term variability and extreme events. J Clim. [accessed 2021 Aug 1];31:1921–1942. *https://doi.org/10.1175/JCLI-D-17-0376.1*

Luković J, Chiang JCH, Blagojević D, Sekulić A. 2021. A later onset of the rainy season in California. Geophys Res Lett. [accessed 2021 Aug 1];48. *https://doi.org/10.1029/2020GL090350*

Meko DM, Stockton CW, Boggess WR. 1980. A tree-ring reconstruction of drought in southern California. J Am Water Resour Assoc. [accessed 2021 Aug 1];16:594–600. *https://doi.org/10.1111/j.1752-1688.1980.tb02436.x*

Meko D. 1981. Applications of Box–Jenkins methods of time series analysis to the reconstruction of drought from tree rings [dissertation]. [Tucson(AZ)]: The University of Arizona. 149 p.

Meko DM, Baisan CH. 2001. Pilot study of latewood-width of conifers as an indicator of variability of summer rainfall in the North American monsoon region. Int J Climatol. [accessed 2021 Aug 1];21:697–708. *https://doi.org/10.1002/joc.646*

Meko DM, Therrell MD, Baisan CH, Hughes MK. 2001. Sacramento river flow reconstructed to A.D. 869 from tree rings. J Am Water Resourc Assoc. [accessed 2021 Aug 1];37;1029–1039. *https://doi.org/10.1111/j.1752-1688.2001.tb05530.x*

Meko DM, Woodhouse CA. 2005. Tree-ring footprint of joint hydrologic drought in Sacramento and Upper Colorado river basins, western USA. J Hydrol. [accessed 2021 Aug 1];308:196–213. *https://doi.org/10.1016/j.jhydrol.2004.11.003*

Meko DM, Stahle DW, Griffin D, Knight TA. 2011. Inferring precipitation-anomaly gradients from tree rings. Quat Int. [accessed 2021 Aug 1];23:89–100. *https://doi.org/10.1016/j.quaint.2010.09.006*

Michaelsen J, Haston L, Davis FW. 1987. 400 years of northern California precipitation variability reconstructed from tree rings. J Am Water Resourc Assoc. [accessed 2021 Aug 1];23:809–818. *https://doi.org/10.1111/j.1752-1688.1987.tb02956.x*

Neelin JD, Langenbrunner B, Meyerson JE, Hall A, Berg N. 2013. California winter precipitation change under global warming in the coupled model intercomparison project phase 5 ensemble. J Clim. [accessed 2021 Aug 1];26;6238–6256. *https://doi.org/10.1175/JCLI-D-12-00514.1*

Polade SD, Gershunov A, Cayan DR, Dettinger MD, Pierce DW. 2017. Precipitation in a warming world: assessing projected hydro-climate changes in California and other Mediterranean climate regions. Sci Rep. [accessed 2021 Aug 1];7. *https://doi.org/10.1038/s41598-017-11285-y*

Powers RF. 1990. *Pinus sabiniana*, Digger Pine. In: Burns RA, Honkala BH, editors. Silvics of North America, Volume 1: Conifers. USDA Handbook 654. Washington (DC): US Government Printing Office.

Schneider U, Hänsel S; Finger P; Rustemeier E, Ziese M. 2022. GPCC full data monthly product version 2022 at 0.5°: monthly land-surface precipitation from rain-gauges built on gts-based and historical data. [accessed 2023 Mar 20]. Federal Ministry for Digital and Transport. *https://doi.org/10.5676/DWD_GPCC/FD_M_V2022_050*

Schwartz M, Hall A, Sun F, Walton D, Berg N. 2017. Significant and inevitable end-of-twenty-first-century advances in surface runoff timing in California's Sierra Nevada. J Hydrometeorol. [accessed 2021 Aug 1];18:3181–3197. *https://doi.org/10.1175/JHM-D-16-0257.1*

St. George S, Ault TR. 2011. Is energetic decadal variability a stable feature of the central Pacific Coast's winter climate? J Geophys Res Atmos. [accessed 2021 Aug 1];116. *https://doi.org/10.1029/2010JD015325*

St. George S, Meko DM, Cook ER. 2010. The seasonality of precipitation signals embedded within the North American Drought Atlas. Holocene. [accessed 2021 Aug 1];20:983–988. *https://doi.org/10.1177/0959683610365937*

Stahle DW, Therrell MD, Cleaveland MK, Cayan DR, Dettinger MD, Knowles N. 2001. Ancient blue oaks reveal human impact on San Francisco Bay salinity. Eos. [accessed 2021 Aug 1];82:141–145. *https://doi.org/10.1029/EO082i012p00141*

Stahle DW, Cleaveland MK, Grission–Mayer HD, Griffin RD, Fye FK, Therrell MD, Burnette DJ, Meko DM, Villanueva Diaz J. 2009. Cool- and warm-season precipitation reconstructions over western New Mexico. J Clim. [accessed 2021 Aug 1];22:3729–3750. *https://doi.org/10.1175/2008JCLI2752.1*

Stahle DW, Griffin RD, Meko DM, Therrell MD, Edmondson JR, Cleaveland MK, Stahle LN, Burnette DJ, Abatzoglou JT, Remond KT, et al. 2013. The ancient blue oak woodlands of California: longevity and hydroclimatic history. Earth Interact. [accessed 2021 Aug 1];17:1–23. *https://doi.org/10.1175/2013EI000518.1*

Stahle DW, Cook ER, Burnette DJ, Torbenson MCA, Howard IM, Griffin D, Villanueva–Diaz J, Cook BI, Williams AP, Watson E, et al. 2020. Dynamics, variability, and change in seasonal precipitation reconstructions for North America. J Clim. [accessed 2021 Aug 1];33:3173–3195. *https://doi.org/10.1175/JCLI-D-19-0270.1*

Steinschneider S, Ho M, Williams AP, Cook ER, Lall U. 2018. A 500-year tree ring-based reconstruction of extreme cold-season precipitation and number of atmospheric river landfalls across the southwestern United States. Geophys Res Lett. [accessed 2021 Aug 1];45:5672–5680. *https://doi.org/10.1029/2018GL078089*

Swain DL, Horton DE, Singh D, Diffenbaugh NS. 2016. Trends in atmospheric patterns conducive to seasonal precipitation and temperature extremes in California. Sci Adv. [accessed 2021 Aug 1];2. *https://doi.org/10.1126/sciadv.1501344*

Swain DL, Langenbrunner B, Neelin JD, Hall A. 2018. Increasing precipitation volatility in twenty-first-century California. Nat Clim Chang. [accessed 2021 Aug 1];8:427–433. *https://doi.org/10.1038/s41558-018-0140-y*

[USGS] United States Geological Survey. 1958. Summary of floods in the United States during 1958. US Geological Survey Water-Supply Paper 1660-B. [accessed 2023 Mar 20]. Washington, DC: US Government Printing Office. 104 p. Available from: *https://pubs.usgs.gov/wsp/1660b/report.pdf*

Watson E, Luckman BH. 2016. An investigation of the snowpack signal in moisture-sensitive trees from the Southern Canadian Cordillera. Dendrochronologia. [accessed 2021 Aug 1];38:118–130. *https://doi.org/10.1016/j.dendro.2016.03.008*

Welch G, Bishop G. 2006. An introduction to the Kalman filter. [accessed 2023 Mar 20]. Chapel Hill (NC): Dept. of Computer Science, University of North Carolina. Available from: *https://www.cs.unc.edu/~welch/media/pdf/kalman_intro.pdf*

Williams AP, Abatzoglou JT, Gershunov A, Guzman–Morales J, Bishop DA, Balch JK, Lettenmaier DP. 2019. Observed impacts of anthropogenic climate change on wildfire in California. Earth's Future. [accessed 2021 Aug 1];7:892–910. *https://doi.org/10.1029/2019EF001210*

Williams AP, Anchukaitis KJ, Woodhouse CA, Meko DM, Cook BI, Bolles K, Cook ER. 2021. Tree rings and observations suggest no stable cycles in Sierra Nevada cool-season precipitation. Water Resourc Res. [accessed 2021 Aug 1];57. *https://doi.org/10.1029/2020WR028599*

Willis AD, Lund JR, Townsley ES, Faber BA. 2011. Climate change and flood operations in the Sacramento Basin, California. San Franc Estuary Watershed Sci. [accessed 2021 Aug 1];9(2). *https://doi.org/10.15447/sfews.2011v9iss2art3*

Wise EK. 2020. Sub-seasonal tree-ring reconstructions for more comprehensive climate records in US West Coast watersheds. Geophys Res Lett. [accessed 2021 Aug 1];48:e2020GL091598. *https://doi.org/10.1029/2020GL091598*

Woodhouse CA, Meko DM, Bigio ER. 2020. A long view of southern California water supply: perfect droughts revisited. J Am Water Resourc Assoc. [accessed 2021 Aug 1];56:212–229. *https://doi.org/10.1111/1752-1688.12822*

Ziaco E. 2020. A phenology-based approach to the analysis of conifers intra-annual xylem anatomy in water-limited environments. Dendrochronologia. [accessed 2021 Aug 1];59. *https://doi.org/10.1016/j.dendro.2019.125662*

NOTES

Mock, C. 2019. In-person conversation with D. Stahle in February 2019 discussing the 1862 flood year.